PCCP



PAPER View Article Online



Cite this: DOI: 10.1039/d1cp01666k

Contrasting effect of 1-butanol and 1,4-butanediol on the triggered micellar self-assemblies of C₁₆-type cationic surfactants†

Vinod Kumar,^a Rajni Verma,^b Dwarkesh Satodia,^a Debes Ray, och Ketan Kuperkar, och *Vinod Kumar Aswal, och Katie R. Mitchell-Koch and Pratap Bahadur^d

The self-assembly in aqueous solutions of three quaternary salt-based C₁₆-type cationic surfactants with different polar head groups and identical carbon alkyl chain viz., cetylpyridinium bromide (CPB), cetyltrimethylammonium tosylate (CTAT), and cetyltriphenylphosphonium bromide (CTPPB) in the presence of 1-butanol (BuOH) and 1,4-butanediol (BTD) was investigated using tensiometry, 2D-nuclear Overhauser enhancement spectroscopy (2D-NOESY) and small angle neutron scattering (SANS) techniques. The adsorption parameters and micellar characteristics evaluated at 303.15 K distinctly showed that BuOH promotes the mixed micelle formation while BTD interfered with the micellization phenomenon. The SANS data fitted using an ellipsoid (as derived by Hayter and Penfold using the Ornstein-Zernike equation and the mean spherical approximation) and wormlike micellar models offered an insight into the micelle size/shape and aggregation number (N_{agg}) in the examined systems. The evaluated descriptors presented a clear indication of the morphology transition in cationic micelles as induced by the addition of the two alcohols. We also offer an investigation into the acceptable molecular interactions governing the differences in micelle morphologies, using the non-invasive 2D-NOESY technique and molecular modeling. The experimental observations elucidated from computational simulation add novelty to this work. Giving an account to the structural complexity in the three cationic surfactants, the molecular dynamics (MD) simulation was performed for CPB micelles in an aqueous solution of alcohols that highlighted the micelle solvation and structural transition, which is further complemented in terms of critical packing parameter (PP) for the examined systems.

Received 17th April 2021, Accepted 7th August 2021

DOI: 10.1039/d1cp01666k

rsc.li/pccp

1. Introduction

Cationic surfactants display a wide range of applications in pharmaceuticals, dyeing, enhanced oil recovery, foaming, formulating stable colloidal dispersions and in personal care products due to their excellent adsorption and micellar characteristics. ^{1–3} Studies have reported that colloid-chemical behavior and antistat/antimicrobial properties can be modulated substantially in the presence of additives such as salts, acids,

solvents, surfactants and polymers to enhance their performance in solution. $^{4-9}$

Especially, the alcohols have been expedient in aqueous surfactant systems for their role in tuning the micellar/microemulsions characteristics. Several researchers have examined the modulation of surfactant solution by alcohols to evolve shape and structural transitions in micelles. 10-15 It has been well accepted that short-chain *n*-alcohols (C_nOH , $n \leq 3$) reside in the bulk phase and often disintegrate micelles resulting in loose structures of aggregates while medium-chain alcohols $(C_nOH, n = 4, 5)$ display a partition between the micellar and bulk phases. The micelle-bound higher-chain alcohols reflect as co-surfactants (C_nOH , $n \ge 6$) which intercalate into the ionic micelle and reduce the overall surface charge density. This tends to make them solubilize within the micellar core where the polar head group of alcohol protrudes towards the micellar surface and facilitates micelle formation/growth that leads to viscous solution, higher aggregation number (N_{agg}) and induces microstructural changes in mixed surfactant-alcohol

^a Department of Chemistry, Sardar Vallabhbhai National Institute of Technology (SVNIT), Surat 395007, Gujarat, India. E-mail: ketankuperkar@gmail.com

^b Department of Chemistry, Wichita State University (WSU), Wichita Kansas 67260-0051, USA

^c Solid State Physics Division, Bhabha Atomic Research Centre (BARC), Mumbai 400 085, Maharashtra, India

^d Department of Chemistry, Veer Narmad South Gujarat University (VNSGU), Udhana-Magdalla road, Surat 395007, Gujarat, India

 $[\]dagger$ Electronic supplementary information (ESI) available. See DOI: 10.1039/d1cp01666k

systems. $^{16-20}$ Such a contrasting behavior by short/long chain n-alcohols revealed their partitioning conduct and site in the micelles that influence the solvent properties. In the case of 1,2-diols and α,ω -diols, the former with 4C and higher methylene chains showed greater penetration ability in the micelles, while the latter (even those with a 6–8C long chain) preferred to stay at the micelle surface. 10,12,21,22

Among these alcohols, the medium-chain alcohols (4C) are typically used as co-surfactants or co-solvents. 11,16,17,23 González-Pérez et al. have explained the solubilization of 1-butanol (BuOH) in an aqueous micellar solution of dodecyldimethylethylammonium bromide as a function of temperature by conductivity measurements and found a U-shaped curve of critical micelle concentration (CMC) against temprature.24 Kuperkar et al. studied the interaction of BuOH with cetyltrimethylammonium bromide (CTAB) and suggested that BuOH may encapsulate in the CTAB micelles undergoing a plausible micellar growth.16 Chavda et al. offered quantitative and qualitative effects of partitioning of BuOH and 1,4-butanediol (BTD) in cationic micelles; BuOH partitioned between the micellar phase and the bulk phase while the BTD mainly located in the bulk phase. 17 Maria et al. investigated the solubilization of a series of α,ω-alkanediols in the micellar phase of SDS and DTAB and inferred that the degree of solubilization increases with an increase in the hydrophobicity of alkanediols. 10 Such addition of various alcohols to aqueous surfactant solutions has allowed the researchers to actively investigate the effect of hydrophobic interactions leading to structural changes. 10,12,25,26

Additionally, theoretical investigations depict the behavior of surfactants in the presence of additives. The computational simulations offer insight into the micellar shape/transition and interfacial properties at the molecular level. In addition, the molecular dynamics (MD) simulation findings are found to be consistent with the experimental findings but they can forecast the contrast pattern in experiments and modeling for the counterion affinity with the surfactant head group.²⁷ The MD conducted on cationic micelles in the presence of alcohols offer the most straightforward approach.²⁸⁻³⁰ Rajni et al. studied the atomistic-level analysis of the CPB cationic surfactant for MD simulations which was further validated by studying its structural and dynamic properties in water, 1-octanol, and micelle.²⁸ MD simulations used by Xiangfeng et al. investigated the shape and structural evolution of pre-assembled cylindrical CTAB micelles caused by octanol.²⁹ However, MD simulation studies have scarcely focused on exploring the quantitative effects of alcohol on different cationic micelles.²⁸⁻³⁰

The effect of BuOH and BTD on CMC and aggregation number ($N_{\rm agg}$) of cationic micelles is often ambiguous and depends on the concentration of alcohol and carbon chain/concentration of the surfactant. Hence, we have used three cationic surfactants with 16-carbon alkyl chain length and different polar head groups and counterions viz., cetyltrimethylpyridinium bromide (CPB), cetyltrimethylammonium tosylate (CTAT) and cetyltriphenylphosphonium bromide (CTPPB) to examine the influence of these alcohols (at fixed 1 M concentration) in aqueous solution. Small angle neutron

scattering (SANS) measurements were performed to substantiate the structural parameters of the cationic micelles. The scattering data were interpreted by fitting to an ellipsoidal micelle model for CPB and CTPPB, and to a worm-like micellar model for CTAT. Here, the ellipsoidal micelles are expected to be similar to the spherical micelles for simplification. Two-dimensional nuclear Overhauser enhancement spectroscopy (2D-NOESY) has been used to gather information on the solubilization sites of alcohol molecules in micelles considering the significant and positive cross-peaks in the spectra. More specifically, this work validates the experimental findings using series of simulations to portray the molecular interactions involved in surfactantalcohol systems through the semi-empirical method calculations along with MD simulation analysis using radial distribution functions (RDF), radius of gyration (R_g) and solvent-accessible surface area (SASA), which probe the microstructural evolution involved in the examined CPB-alcohol system. The simulation data are further substantiated with molecular packing analysis.

2. Experimental section

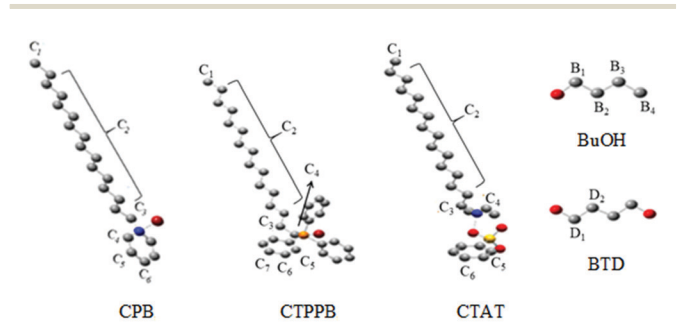
2.1 Materials

The C_{16} -type cationic surfactants νiz ., cetylpyridinium bromide (CPB), cetyltriphenylphosphonium bromide (CTPPB), cetyltrimethylammonium tosylate (CTAT), 1-butanol (BuOH) and 1,4-butanediol (BTD) were purchased from Sigma Aldrich, USA. The optimized structures of the used ingredients are presented in Scheme 1.

Double-distilled water (conductivity \sim 2–4 μS) was used for sample preparation but deuterium oxide (D₂O) (from Sigma, India) was used for SANS and NMR experiments.

2.2 Methods

2.2.1 Tensiometry. Critical micelle concentration (CMC) values of surfactants in water, 1 M BuOH, and 1 M BTD were determined using a Krüss K9 tensiometer following the platinum "du Nouy" ring method at room temperature. The adsorption parameters at the air–water interface νiz ., minimum area per molecule ($A_{\rm min}$), maximum surface excess ($\Gamma_{\rm max}$), and surface pressure at CMC ($\pi_{\rm CMC}$) were evaluated using the Gibbs adsorption equation. ^{31,32}



Scheme 1 Optimized structures of cationic surfactants and alcohols. Here, the labels are addressed to respective protons for 2D-NOESY interpretation.

2.2.2 Small angle neutron scattering (SANS). The neutron scattering data were collected in the range of 0.017–0.35 Å $^{-1}$ at 303.15 K using SANS diffractometer, Dhruva reactor, BARC, India. Here, the data are expressed as absolute intensity versus the accessible scattering wave vector ($Q=4\pi\sin\theta/\lambda$, where 2θ is the scattering angle). The position-sensitive detector (PSD) permits simultaneous data recording over the full Q-range. All the measured scattering distributions were corrected for the background and solvent contribution and normalized to the cross-sectional unit using standard procedures. Here

For the ellipsoidal micelle model, the expression derived by Hayter and Penfold using the Ornstein-Zernike equation and the mean spherical approximation was used. 16,35 For worm-like micelles, the chain of contour length L (total length) can be described by a chain of some number of locally stiff segments (length $l_{\rm p}$). Here, the persistence length $(l_{\rm p})$ is the length along with the cylinder over which the flexible cylinder is considered as a rigid rod. The Kuhn length (b) used in the model also describes the stiffness of a chain and is $b=2l_{\rm p}$. 36

2.2.3 Two dimensional-nuclear Overhauser enhancement spectroscopy (2D-NOESY). The 2D-NOESY experiments were performed using Bruker AVANCE-II 400 MHz spectrometer at St. Francis Xavier University, Antigonish, Canada. The mixing and the delay times for the experiments were estimated from the spin–lattice relaxation times (T_1 values) in cationic surfactants with varying alcohol concentration. In all cases, the acquisition delays of $\approx 3 \times T_1$ and a mixing time of $\approx 1 \times T_1$ were used to obtain the 2D-NOESY spectra. All experiments were done in phase-sensitive mode, with and without the saturation of the water resonance at ~ 4.70 ppm. The data were zero-filled twice in

dimension 1 and multiplied by a squared sine function in both dimensions before 2DFT. ^{16,17}

2.2.4 Computational simulation. The semiempirical method with the PM6 level of Gauss View 5.0.9 package was used to assess the information about the chemical structure and electronic distributions in the individual cationic surfactants, alcohols and the tested surfactant-alcohol systems (Fig. 1). With this, various quantum chemical descriptors like the total energy (TE) associated with the highest occupied molecular orbital (HOMO) and the lowest unoccupied molecular orbital (LUMO) along with the energy gap ($\Delta E = E_{\rm LUMO} - E_{\rm HOMO}$) were evaluated.³²

In addition, we have used molecular dynamics (MD) simulation to gain an insight into the solvation and structural properties of CPB micellar aggregate (only) in 1 M aqueous alcohols. Performing atomistic simulation of CTPPB micelle was troublesome due to the three bulky phenyl rings present in its chemical structure, while the micellar concentration of the CTAT micellar aggregate (20 mM) was too small to observe any significant micellar transitions in the simulations. For MD initiation, the ellipsoidal aggregate of 66 monomers was prepared using Packmol software;³⁷ the GROMOS96 54a7³⁸ forcefield of the CPB molecule reported by Verma *et al.* was used²⁸ and Forcefields of BuOH and BTD were adopted from Automated Topology Builder.^{39,40} The details of the simulation are summarized in Table 1.

The CPB micelle was centered in a ~ 10.5 nm cubic box of aqueous solution to perform the MD simulation at 303 K temperature. BuOH/BTD molecules were randomly placed in the simulation box for simulations in a water-alcohol mixture. The system was first energy minimized for 10 000 steps using

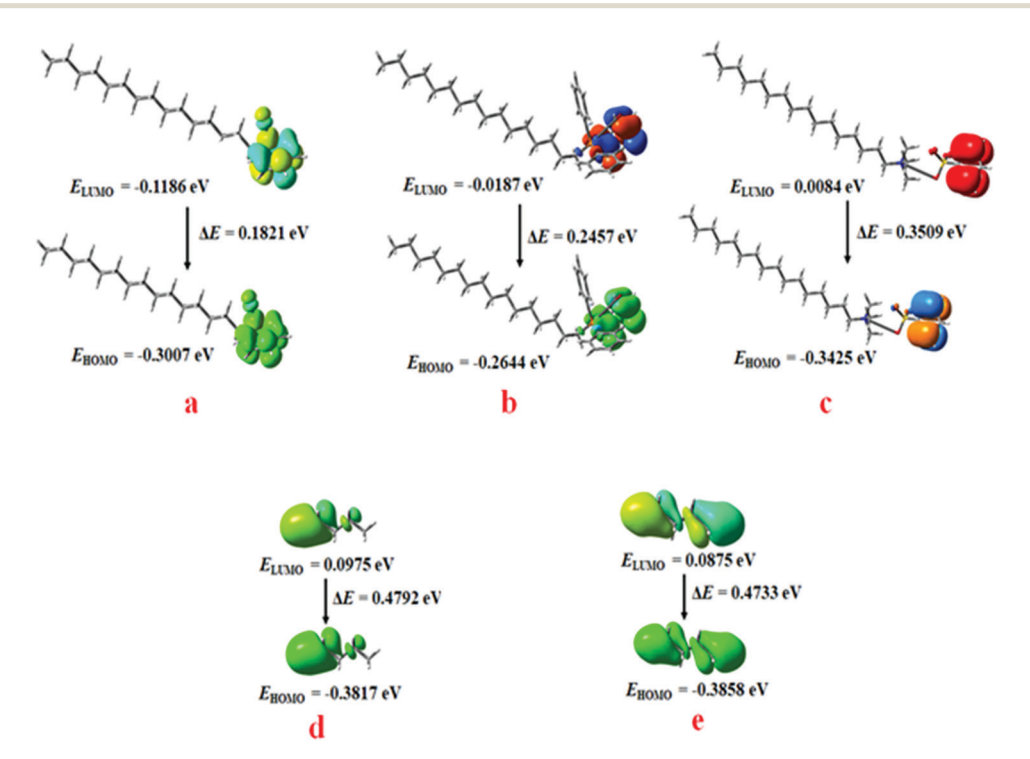


Fig. 1 Optimized structure depicting the HOMO-LUMO orbitals evidenced for individual (a) CPB, (b) CTPPB, (c) CTAT, (d) BuOH, and (e) BTD.

Table 1 Simulation summary of a CPB micelle in solution

System	CPB micelle	Water molecules	Surfactant molecules		Total number of atoms
1	Water	37 218	0	66	113172
2	1 M BuOH	34 392	650	66	108594
3	1 M BTD	33 959	650	66	108595

the steepest descent algorithm in order to remove bad clashes between the atoms. After energy minimization, all the atoms were given an initial velocity obtained from a Maxwellian distribution at 303 K. A time step of 2 fs was used to integrate the equations of motion for all the simulations. First, the system was equilibrated for 50 ps by applying position restraints to the heavy atoms of the CPB molecules for solvent relaxation in the simulation box. Then the position restraints were removed, and the system was gradually heated from 50 K to 303 K during 200 ps of the simulation. After equilibration, a production run of 50 ns was performed for the CPB micelle simulations in water, 1 M BuOH and 1 M BTD using Gromacs 2016.6.

3. Results and discussion

The aqueous solution performance for the selected three cationic surfactants at 30 °C has been reported by several groups, which is higher than their respective Kraft temperature (KT). Here, the KT of CPB, CTPPB and CTAT is around 29.3 °C, not reported, and 23.0 °C respectively. 42,43 Giving an account of their structural complexity in terms of the bulky polar head groups and counterions, the degree of the hydrophobicity followed the order: CTPPB > CPB > CTAT which influenced their micellization and aggregation ability i.e., CMC for CPB, CTPPB and CTAT in water was found to be 0.80 mM, 0.40 mM and 0.24 mM respectively. 44-47 In addition, for the selected two different solvents, BuOH and BTD with varying hydrophobicity i.e., BuOH > BTD, various properties such as partition coefficient ($log P_{o/w}$), water solubility and dielectric constant were reported as 0.88, 10 mg mL⁻¹ (at 20 °C), and 17.84 (at 20 °C) for BuOH and -0.83, completely miscible, 31.63 (at 20 $^{\circ}$ C) for BTD. 23,48

3.1 Tensiometry

According to the Gibbs equation, the charged surfactants tend to adsorb at the air-water interface to form a charged adsorption film that captures the counterions with the surfactant opposite charge, resulting in the reduction of surface tension (ST). The characteristic semi-logarithmic ST (γ) plots for the surfactant at different concentrations over pre- and post-micellar regions are constructed as shown in Fig. 2. An initial slow decrease in ST at a very low concentration followed by a steep fall in accordance to Gibbs adsorption isotherm and finally attaining a constant value with an intersection point depicting the CMC are typical of surfactant behavior. The CMC of CPB (\sim 0.79 mM) in water agree with the reported value. ⁴⁴ The lower CMC of CTAT (\sim 0.32 mM) is due to strong binding to the sylate counterion and that of CTPPB (\sim 0.37 mM) is due

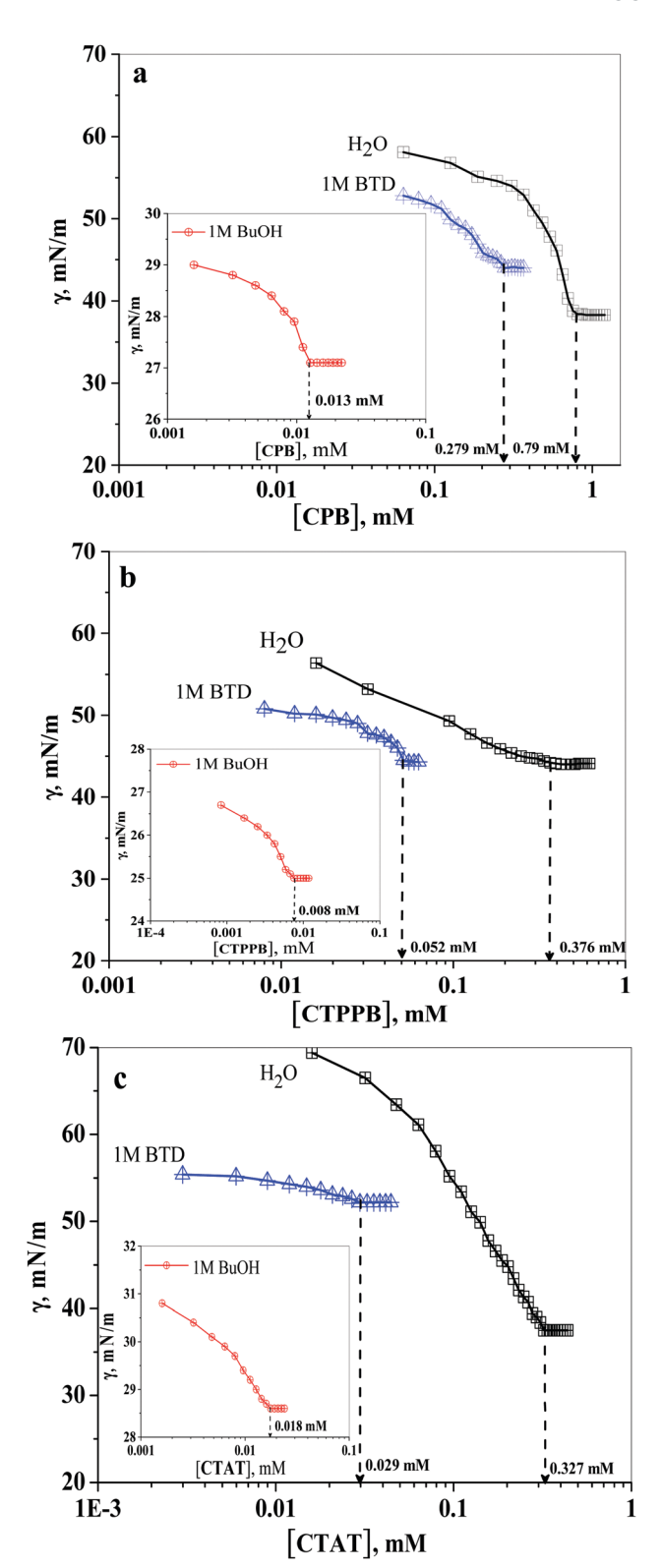


Fig. 2 Surface tension (ST) curves for surfactants in water, 1 M BuOH (inset plot) and 1 M BTD alcohols at 303.15 K. Arrows in the plot indicate the CMC of the respective surfactants in the selective solvent.

to a highly hydrophobic polar head group despite its large size as also reflected in the high $\gamma_{\rm CMC}$ (~44.2 mN m⁻¹) values and higher $A_{\rm min}$ (229.1 Å²).^{45,46}

PCCP Paper

For each surfactant in 1 M BuOH, the ST showed a much larger decrease even at the lowest surfactant concentration and depicts lower γ_{CMC} and CMC compared to that in water (data shown in the ESI,† Table S1). This shows that BuOH behaves as a co-solvent and co-surfactant for each tested surfactant which is quite customary. However, BTD acts as a co-solvent showing typical behavior for all three surfactants. Lower ST, higher $\gamma_{\rm CMC}$ values and decreased CMC in comparison to water can be clearly noticed from ST-concentration plots (Fig. 2). It was observed that the CMC decrease by BTD is not as remarkable as observed for BuOH which infers that the more hydrophobic the alcohol is, the greater the decrease in CMC and γ_{CMC} . The BTD molecules being very hydrophilic with two terminal -OH groups of 4C chain, don't penetrate inside the micelle, instead they reside on the surface close to the polar head groups of the micelles and alter the solvent (water) properties and there is no marked effect on the CMC.

The increase in CMC by short chain alcohols (C_nOH , $n \leq 3$) and other miscible polar solvents results from the decrease in dielectric constant and decreased hydrophobic interaction. A drop in CMC may result when the polar additives molecules adsorb on the micelle surface or slightly penetrate in micelles thereby decreasing the electrical repulsion between the polar head groups. The CMC can slightly increase/decrease in the case of BTD, which may be due to these opposing effects and depends on its concentration and the structure of surfactant. The slight increase in CMC for the cationic surfactant in the presence of BTD has been observed by Chavda¹⁷ et al. and Tomi²¹ et al. BuOH being more hydrophobic adsorbs on the air-water interface along with the surfactant and penetrates inside the micelle and therefore exerts a larger decrease in CMC and $\gamma_{\rm CMC}$ as well as higher area per molecule ($A_{\rm min}$) occupied by the surfactant at the air-water interface at closest packing due to the reduced electrostatic repulsion and enhanced hydrophobic interaction. Such behavior goes well with a previously reported study.⁴⁹ The π_{CMC} values increase in the presence of 1 M BuOH, which indicates stronger adsorption of the surfactants at the air-water interface whereas the same was observed to decrease in the presence of 1 M BTD which is due to its reduced surface activity. The $\Gamma_{\rm max}$ of surfactants in water decreases more in the presence of BuOH than BTD, which reflects a favorable degree of interfacial saturation in the former thereby solubilizing the respective alcohol in surfactant micelles (data shown in the ESI,† Table S1). Thus, BuOH promotes the mixed-micelle formation while BTD interfers with the micellization.

3.2 Scattering utline

The SANS findings offer a quantitative evaluation depicting the influence of alcohols on the modulated geometry of cationic surfactant micelles. 16,17 Fig. 3 displays the normalized peak intensity, which decreases in the presence of BuOH and BTD. The later observations clearly indicate that the -OH group of alcohol gets more interspersed between the charged surfactant head groups and facilitates the alcohol solubilization within the micelles. Furthermore, the decrease in the intermicellar distance within the examined system successively corroborates

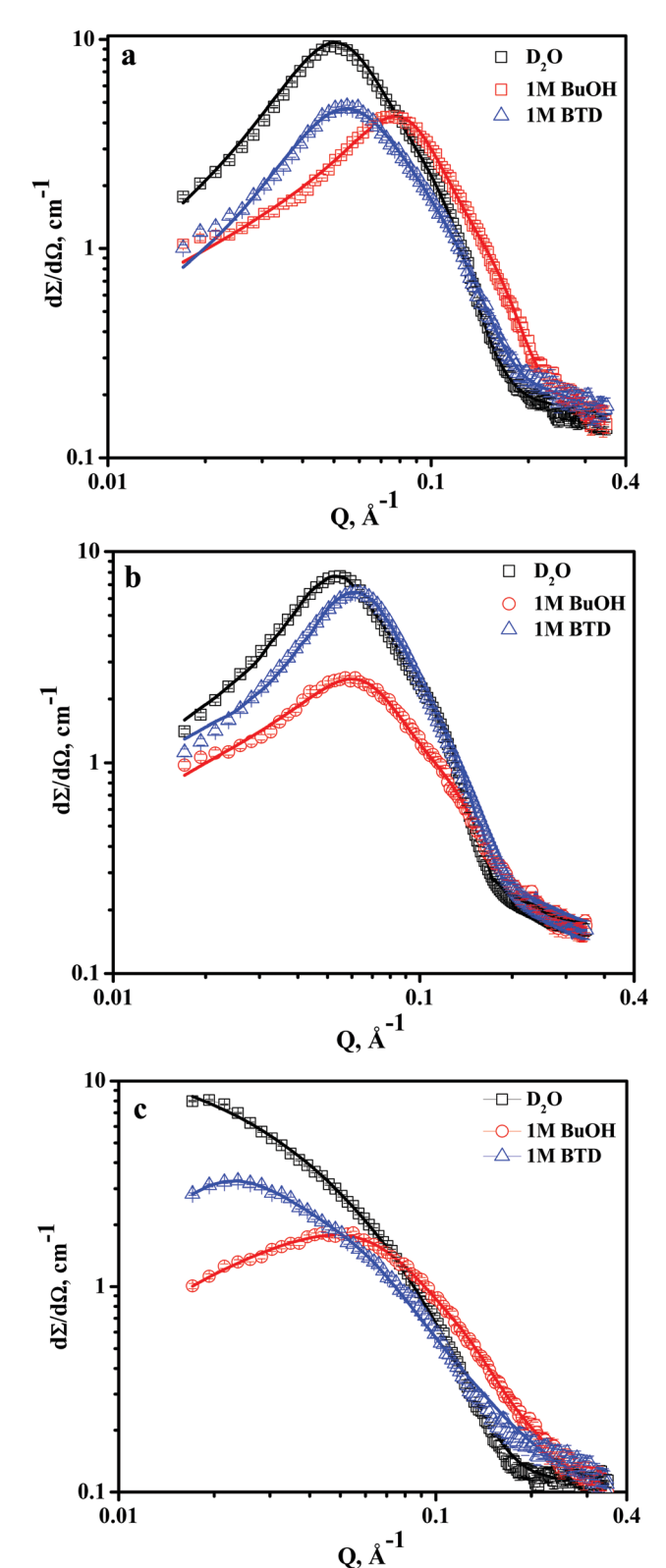


Fig. 3 SANS sketch of (a) 100 mM CPB, (b) 100 mM CTPPB and (c) 20 mM CTAT in D₂O, 1 M BuOH and 1 M BTD at 303.15 K.

the shifting in the correlation peaks towards a higher Q region which seem to be more pronounced in the presence of BuOH than BTD.

Table 2 reveals that 100 mM CPB and CTPPB display ellipsoidal micellar geometry while 20 mM CTAT exhibits a worm-like micelle. As reported, $N_{\rm agg}$ supports the idea of micellar growth. Here, it was observed that $N_{\rm agg}$ decreases more in the presence of BuOH than BTD. Such behavior by the former enables it to act as a short chain length alcohol that confers its favorable solubility tendency near the hydrophobic tail region of each cationic surfactant in comparison to the latter. This finding is well supported by the reported literature. It is finding is well supported by the reported literature. Also, it is expected behavior of BTD, in which it is taken into account where it does not partition very well within micelles. Thus, adding BTD simply changes the solvent structure, resulting in lower $N_{\rm agg}$. 10,12,52

3.3 Spectral outline

Giving an account of the labels addressed in Scheme 1 and Fig. 4 exhibits a fair number of cross-peaks that provide enough evidence about the solubilization loci and the extent of interaction of both the alcohols in respective cationic surfactant micelles.

CPB in BuOH and BTD. 2D-NOESY spectra for CPB in 3.3.1 the presence of BuOH showed strong correlation peaks between the carbon terminal-chain protons of CPB (C₁ and C₂) and BuOH (B₂, B₃ and B₄) in the region of ~ 0.5 to ~ 1.7 ppm. Furthermore, the interaction between B₁ protons of BuOH and C_1 and C_2 protons of CPB was noticed around ~3.60 ppm. These observations concluded that the -OH group of BuOH is located near the outer shell of the CPB micelle. Also, the 2D-NOESY spectra for the CPB-BTD system displayed cross-peaks between the D₁ proton of BTD and the C₂ proton of CPB at \sim 3.60 ppm. However, we could not find any other intense cross-peak between tail protons of CPB and BTD which clearly indicates that there is a strong correlation between the polar head group of CPB and BTD, leading to BTD residing at the micelle surface, as opposed to it penetrating the CPB micelle core.

3.3.2 CTPPB in BuOH and BTD. Similarly, the 2D-NOESY spectra of CTPPB in the presence of BuOH showed intense overlapping cross-peaks observed for the internal and terminal chain protons of CTPPB (C_1 , C_2 and C_3) and BuOH (B_2 , B_3 and B_4) (between ~ 0.5 –2.0 ppm) depicting a strong collaboration between them. Furthermore, intense cross-peaks between the B_1 protons of BuOH with a tail proton of CTPPB are observed at ~ 3.5 ppm.

This observation is attributed to the BuOH molecule interacting more with the non-polar tail of the surfactant and remaining vested within the micelle, such that the –OH group protrudes outside the micelle and the 4 carbon chain is oriented towards the micelle core. The weak cross-peak between ~ 0.5 –2.0 ppm is observed for CTPPB and BTD, which indicates BTD remains near the micelle surface, not in the micellar core. In addition, the spectra displayed cross-peaks between the D_2 proton of BTD and the C_4 proton of CTPPB at ~ 3.60 ppm, which indicates that BTD persists at the micelle surface, thereby preventing its penetration into the CTPPB micelle core.

3.3.3 CTAT in BuOH and BTD. Likewise, the 2D-NOESY spectra for CTAT-BuOH showed correlation peaks between the terminal carbon chain protons (C₁ and C₂) of CTAT and B₂, B₃ and B_4 protons of BuOH in the region of ~ 0.5 to ~ 1.7 ppm. Such an observation indicates that BuOH interacts with the CTAT micelle where the -OH group is found in proximity with a head group of CTAT. This is supported by cross-peaks between the head protons of CTAT and the hydroxyl proton of BuOH at \sim 3.50 to \sim 3.60 ppm. Furthermore, the intense cross-peaks between both the D₁ proton of BTD and the C₂ proton of CTAT were observed at ~3.50 ppm. A very weak cross-peak at ~ 1.50 ppm showed poor interaction between the terminal chain protons of BTD and CTAT, which is a clear indication that BTD interacts only with the head group of CTAT near the micelle surface and fails to penetrate inside the CTAT micelle core.

These spectral findings were further validated using a simulation approach that supports the indicated molecular interactions between the examined surfactant-alcohol systems in the next section.

3.4 Computational simulation

Fig. 5 indicates the uniform electronic density in the HOMO and LUMO on the entire area of cationic surfactant-alcohol systems which is due to the π -electron cloud density of these systems. A lower HOMO–LUMO energy gap indicates high stability and induces more interaction within the surfactant-alcohol systems.

Fig. 6 show the dynamic behavior of the CPB micellar aggregate (100 mM) during MD simulations in water, 1 M BuOH, and 1 M BTD solution. It was observed that the CPB micelle remains ellipsoidal in the water simulation with an

Table 2 SANS parameters (a = semi-major axis, b = semi-minor axis, R_{hs} = hard sphere radius, ϕ = volume fraction, N_{agg} = aggregation number) for cationic surfactants in different solvent environments at 303.15 K

Surfactant	Solvent	a (Å)	b (Å)	a/b	$R_{ m hs}$ (Å)	ϕ	$N_{ m agg}$	Micelle shape
100 mM CPB	D_2O	33.3	21.5	1.6	51.9	0.20	141	Ellipsoidal
	1 M BTD	29.6	18.1	1.6	47.1	0.20	89	Ellipsoidal
	1 M BuOH	23.9	15.0	1.6	34.5	0.20	49	Ellipsoidal
100 mM CTPPB	D_2O	30.0	20.3	1.5	49.9	0.20	113	Ellipsoidal
	1 M BTD	28.2	18.6	1.5	42.6	0.20	89	Ellipsoidal
	1 M BuOH	26.7	13.3	2.0	43.3	0.15	43	Ellipsoidal
20 mM CTAT	20 mM CTAT D_2O Cross-sectional radius of worm-like micelles $(R_w) = 19.0 \text{ Å}$							Worm-like
	1 M BTD	$R_{\rm w} = 19.0 \text{ Å} \ a = 58.8 \text{ Å}, \ b = 17.5 \text{ Å}$			84.0	0.10	_	Ellipsoidal + worm-like
	1 M BuOH	54.0	12.4	4.4	62.4	0.09	76	Ellipsoidal

Published on 09 August 2021. Downloaded by S.V. National Institute of Technology on 8/28/2021 4:07:12 AM.

PCCP Paper

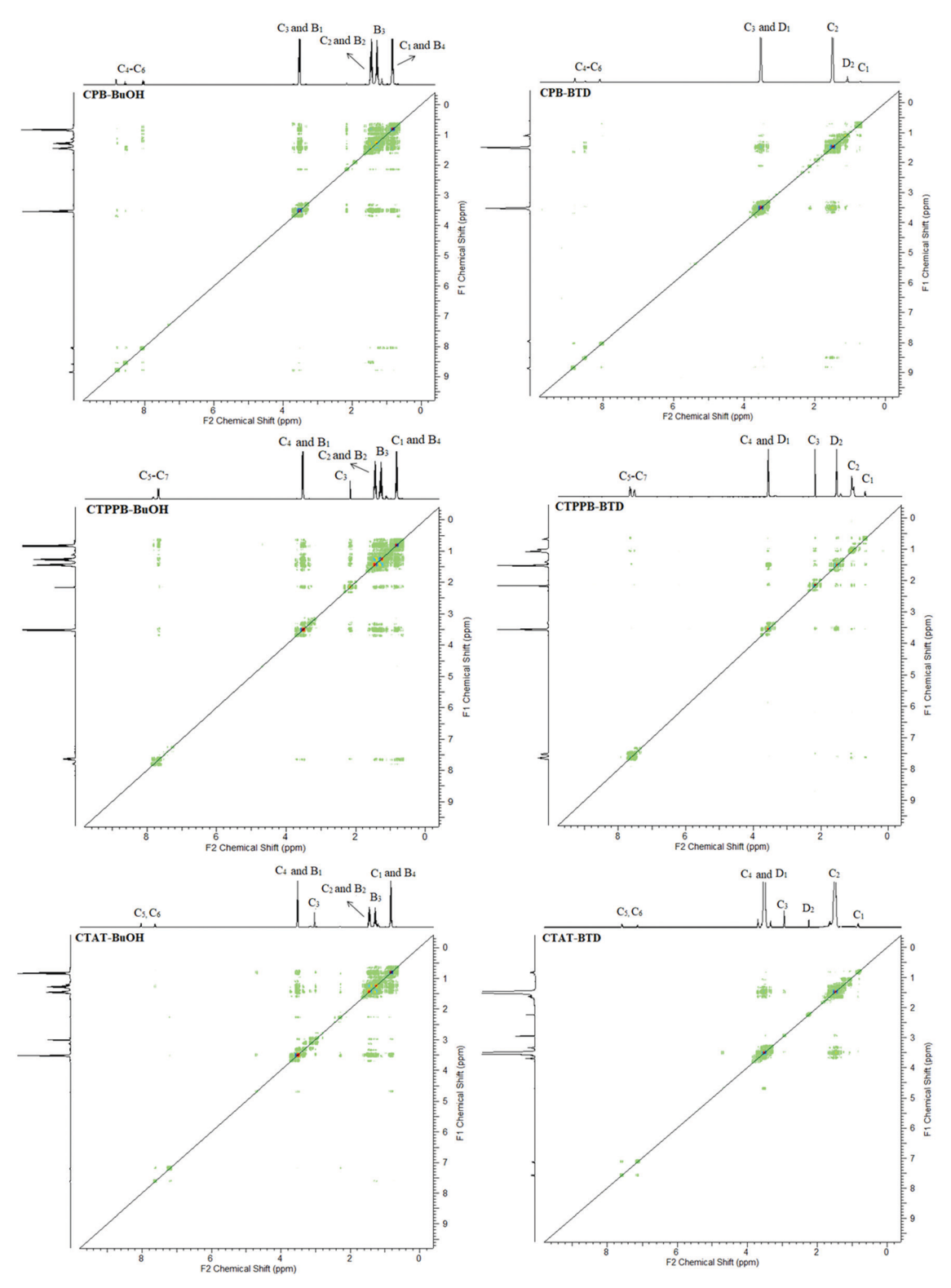


Fig. 4 2D-NOESY profile of cationic surfactants in D₂O solutions containing BuOH and BTD.

average radius of gyration (R_g) of 1.83 \pm 0.02 nm whereas in the water-alcohol mixtures, CPB micelles go through solventinduced changes in shape and size during the first 15 ns to 20 ns of the simulation and then maintain an equilibrated structure afterward. At this stage, the CPB micelle has a higher average $R_{\rm g}$ of 2.65 \pm 0.30 nm in 1 M BuOH solution and 2.02 \pm 0.10 nm in 1 M BTD solution than in water. Thus, simulation results indicate that CPB monomers quickly reorient and rearrange themselves in response to the solvent environment and result in more dynamic behavior.

Paper PCCP

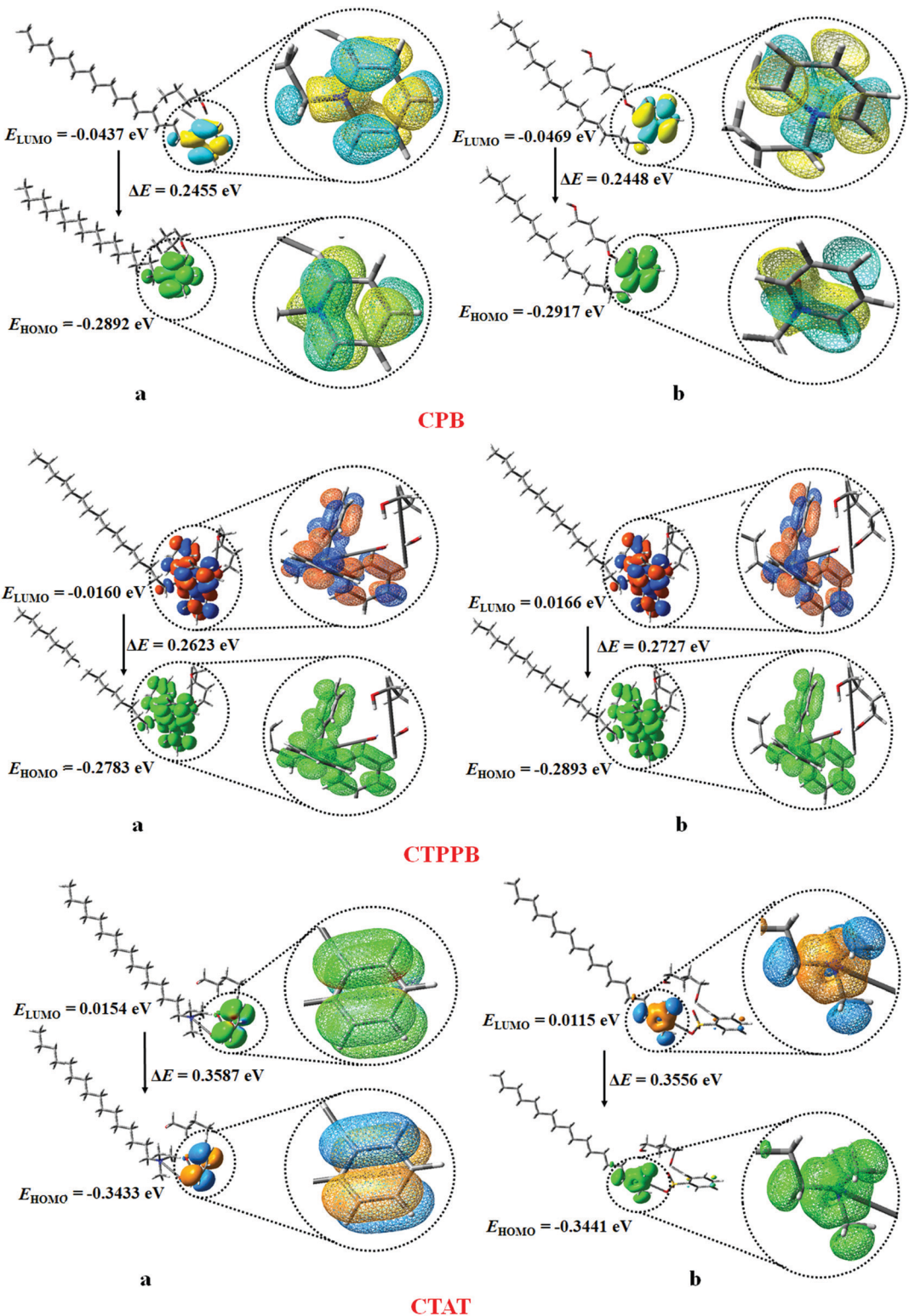


Fig. 5 Optimized structures depicting HOMO-LUMO orbitals for cationic surfactants in (a) BuOH and (b) BTD.

To check further the consistency of such dynamic behavior, we performed simulations with a higher concentration of CPB micelles (162 mM) in water, 1 M BuOH, and 1 M BTD solution and observed a clear micellar transition induced by BuOH and BTD (Fig. 7). Here, the CPB micelles go through the solvent

induced changes in the shape and size in the first 30 ns of the simulation and maintain an equilibrated structure afterward. At this point, the CPB micelle changes from an ellipsoidal shape to an elongated or rod-like micelle with an average $R_{\rm g}$ of 4.18 \pm 0.21 nm in 1 M BuOH solution. However, the CPB

PCCP Paper

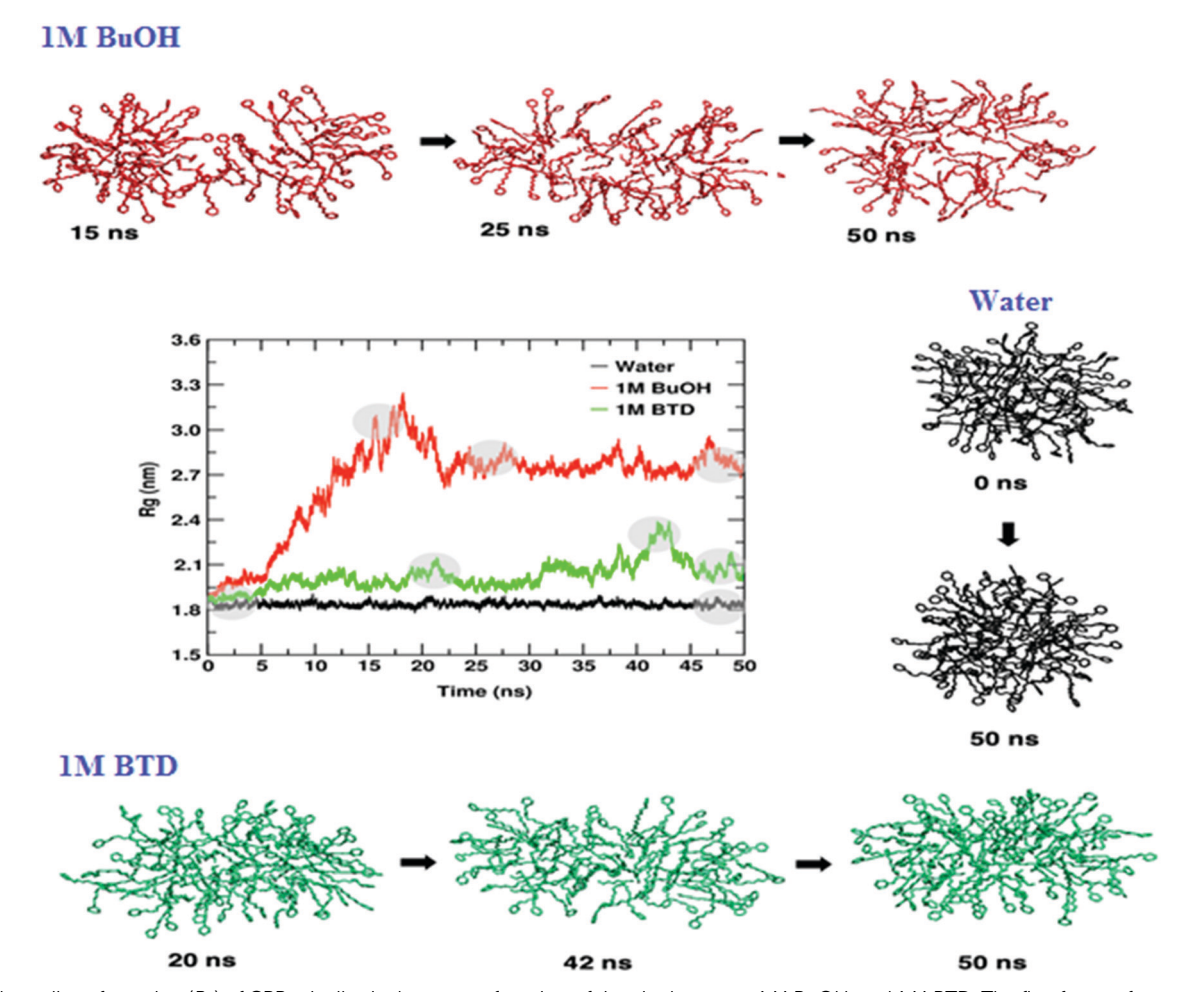


Fig. 6 The radius of gyration (R_0) of CPB micelles is shown as a function of time in the water, 1 M BuOH, and 1 M BTD. The first frame after equilibration, the last frame of 50 ns simulation, and frames showing major changes in R_a during the simulations are shown by the shaded region in the graph and the structure of the CPB micelle in water, 1 M BuOH, and 1 M BTD. The arrow shows the progression of the simulation, with labeled simulation time in ns.

micelles split into two spherical micelles with an average R_g around 2.13 \pm 0.12 nm in 1 M BTD solution. Such simulation findings are attributed to the interaction of alcohol molecules thereby influencing the surface of cationic surfactant aggregates and leading to varied shapes and dynamics.

In addition, the behavior of the CPB micelles is entirely affected by the aqueous solution around them. Solvation of the micelle was assessed using a radial distribution function (RDF) that predicts the average packing of solvent molecules at a distance (0.44 nm) around the CPB micelle. RDF was calculated from the pyridinium N atom of the CPB molecule to the oxygen (O) and hydrogen (H) of water and the hydroxyl group of BuOH and BTD. Fig. 8 shows the probability of solvent density around the pyridinium N in the water, BuOH and BTD. The first and second hydration shells are located at 0.44 nm and 0.56 nm, respectively, for the hydrogen and oxygen of water molecules during the simulations. The average cumulative number of water molecules around CPB in the micelle, within the first solvation shell (0.44 nm) is \sim 5 in water simulation, and \sim 4 in the 1 M BuOH and 1 M BTD simulations. RDF values of the hydration shell indicate a similar distribution of water molecules around the pyridinium ring of the CPB micelle. However, the slightly lower cumulative number of the water molecules around the micelle in 1 M BuOH and BTD solution is due to the interaction of BuOH and BTD molecules with the micelle during the simulations. In BuOH and BTD solvents, the first and second solvation shells were located at 0.33 and 0.42 nm for oxygen and 0.40 nm for hydrogen of the -OH group in the CPB micelle simulations. The RDF of BuOH and BTD around CPB has much higher values than water. Similar behavior in the probability distribution of the RDF peaks of water and 1-octanol around the CPB monomer was observed earlier by Verma et al.²⁸

The high value of the RDF peak of BuOH and BTD is the reflection of the preferential orientation of oxygen in solvating CPB. Even BuOH has a higher RDF peak intensity than BTD, which also supports the fact that the observed density differences are the effects of solvent length and shape. The bromide ion remains at an average distance of 0.5 nm from pyridinium N of CPB during the simulations as observed earlier in the simulations of CPB²⁸ and CTAB micelles.^{53,54}

To understand the hydrophobic and hydrophilic properties of the micellar aggregates in aqueous solution, Fig. 9(a-c)

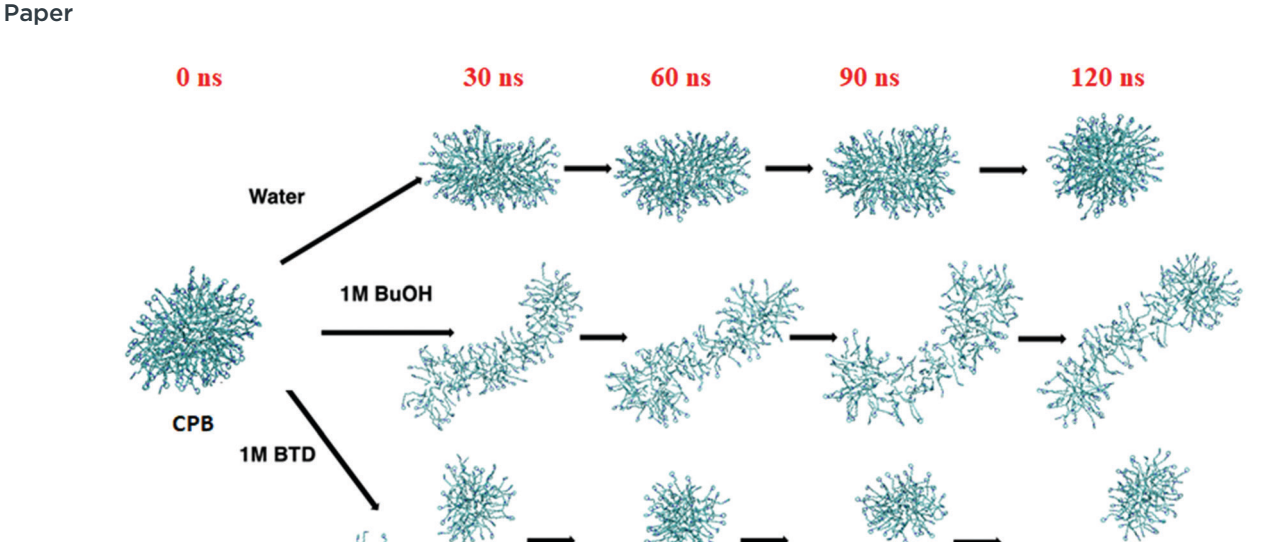


Fig. 7 Snapshots of CPB micelle (162 mM) in water, 1 M BuOH and 1 M BTD starting from conformation after equilibration (0 ns) and in 30 ns intervals up to 120 ns. The arrow shows the progression of the simulation, with the simulation time labeled in ns.

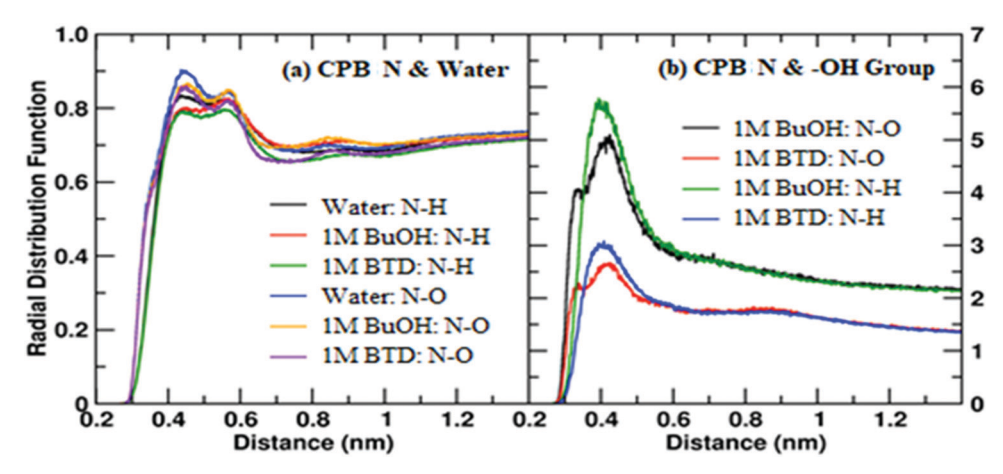


Fig. 8 The RDF for the solvent atoms is shown from the pyridinium N atom of the CPB monomer for (a) water hydrogen and oxygen, and (b) hydroxyl group oxygen and hydrogen around the CPB micelle.

exhibit the calculated the solvent-accessible surface area (SASA) values for the CPB micelle in water, 1 M BuOH, and 1 M BTD solution. In water, the CPB micelle has an average total solvent accessible area of 173 \pm 3 nm² with contribution from the hydrophobic core of 113 \pm 3 nm² and hydrophilic area of 135 \pm 1 nm². After equilibration of 30 ns in BuOH, the total surface area of the CPB micelle increases to 321 \pm 5 nm² (\sim 1.9 fold) with increased exposure of the hydrophobic core to 253 \pm 5 nm² (\sim 2.2 fold) and a hydrophilic area of 137 \pm 1 nm². In 1 M BTD, the CPB micelles have a total area of 204 \pm 7 nm² with a hydrophobic core of 140 \pm 7 nm², and hydrophilic area of 135 \pm 1 nm². Such major changes in the hydrophobic core mainly influence the micelle shape and dynamics due to more favorable solvent interactions in the hydrophilic area. Also, the simulation data indicates how solvent molecules approach the

surface of these aggregates and affect their shape and dynamics. Fig. 9(d-f) show the surroundings of the selected CPB monomer in the micelle using the last frame of simulations. Three CPB monomers exist within 1.2 nm from the pyridinium N of the selected CPB monomer in water (Fig. 9d). However, only two neighboring CPB monomers are found in both 1 M BuOH and BTD solvent environments. Overall, a high number of BuOH molecules were found surrounding the selected CPB molecule compared to the number of BTD molecules in the micellar aggregate.

Thus, the simulation results support the experimental observations of a more favorable interaction of BuOH with a CPB micellar aggregate than BTD, characterized by a greater solubilization tendency of BuOH than BTD near the palisade layer of the cationic micelles.

PCCP Paper

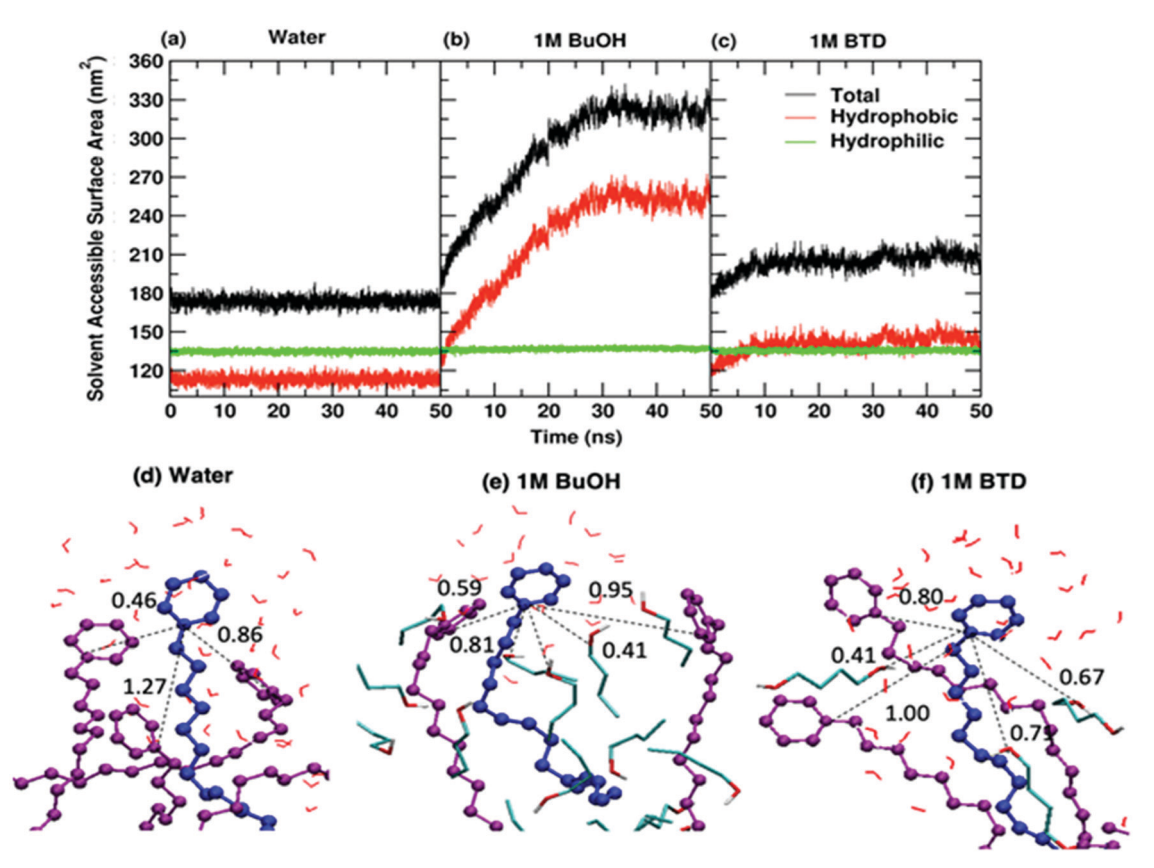
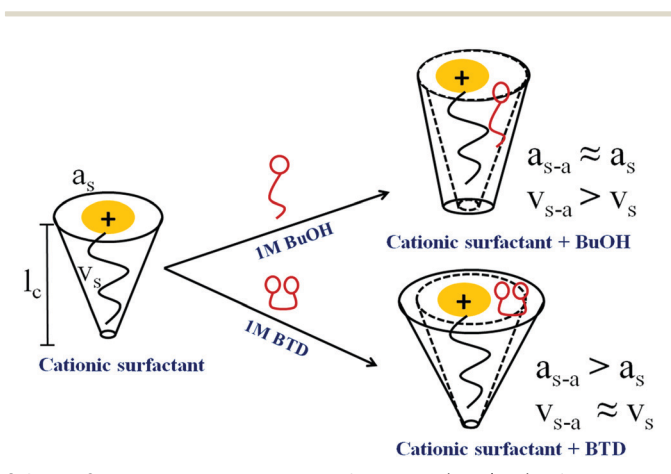


Fig. 9 Solvent accessible surface area (SASA) of the CPB micelle as a function of time in (a) water for the spherical micelle, and in (b) 1 M BuOH and (c) BTD for the elongated micelle. Last frame of the micelle simulation showing residues within 0.5 nm of the selected CPB molecule in blue color in (d) water, (e) 1 M BuOH and (f) 1 M BTD. CPB molecules are in CPK representation and solvent molecules are in licorice representation. Intermolecular distances between pyrimidine N of CPB in the center are shown by dotted lines with the labeled distance in nm.

Based on the MD simulation results, the micellar growth/ transition in cationic surfactants under the influence of alcohols has been well explained in terms of packing parameter (PP), as



Scheme 2 Representation layout of the PP (= v/a_0l_c) of a cationic surfactant in an alcohol system depicting micellar transition. (Here, v_s denotes the volume of the hydrophobic tail for the surfactant, a_s denotes the effective area of the surfactant head group, ls denotes the hydrophobic tail length for the surfactant, $a_{\rm s-a}$ denotes the effective area of the head group for the surfactant-alcohol, and l_s denotes the hydrophobic tail length for the surfactant-alcohol).

shown in Scheme 2. Here, it is evident that the polar shell region $(a_{s-a} \approx a_s)$ remains constant, but the volume of the hydrophobic tail $(v_{s-a} > v_s)$ increases in the presence of BuOH due to its intercalation in the hydrophobic region of the CPB micelle. This outcome increases the PP and changes its curvature which promotes micellar growth. In the case of BTD, the volume of the hydrophobic tail ($v_{\rm s} \approx v_{\rm s-a}$) remains constant, but the polar shell region $(a_{s-a} > a_s)$ increases as BTD interacts more with the head group of surfactants resulting in a decrease in PP and promotes the splitting of the micelle. This behavior is illustrated in the reported work⁵⁵ and is well supported by spectral and simulation studies in Fig. 3 and 6, respectively.

4. Conclusions

The solution behavior of cationic surfactants belonging to the 16-carbon alkyl chain in the presence of BuOH and BTD was demonstrated to favor micellization i.e., the CMC of each surfactant was found to decrease in the presence of these alcohols. The relative adsorption parameters revealed a greater influence of BuOH than BTD, which may be due to the greater solubilization of BuOH relative to BTD, leading to a varied morphology transition. The SANS results showed a similar trend in terms of N_{agg} which was found to decrease.

Furthermore, the shift in the correlation peak of each surfactant towards the high Q region was more profound in the case of BuOH than BTD. The 2D-NOESY experiments offered an insight into the successive and favorable interactions taking into account BuOH and BTD sites in the cationic micellar aggregates. Such behavior is due to the interaction of BTD with the head group of cationic surfactants, while BuOH resides in the palisade region. The molecular orbital calculations using a semiempirical method showed lower ΔE with alcohols reflecting favorable interactions. The MD simulation of the CPB micelle provided a molecular picture of the effect of alcohols on micelle morphology and solvation, with observations of significant structural changes in the micellar aggregates expressed in terms of the R_g , RDF and SASA. The calculated R_g values inferred that the CPB micelle stayed ellipsoidal throughout the simulation and changed to an elongated or rod-like micelle in 1 M BuOH solution, whereas the micelle split into two spherical micelles in the case of 1 M BTD solution. In addition, the measured SASA offered insight into the hydrophobic and hydrophilic properties of the CPB micellar system in aqueous solution where the SASA values of the CPB micelle increased more in the case of BuOH than BTD. The simulation results were found to be consistent with the experimental data showing the significant effect of BuOH and BTD solvation on the structure, dynamics, and aggregation properties of the CPB micelle. These findings are well complemented by the critical PP which makes our surfactantalcohol mix study more useful in industrial applications.

Author contributions

Vinod Kumar: conceptualization, formal analysis, investigation, data collection, writing – original draft, visualization. Rajni Verma and Katie R. Mitchell-Koch: data analysis, validation, writing – review and editing. Dwarkesh Satodia: data collection. Debes Ray and Vinod Kumar Aswal: data analysis and interpretation. Ketan Kuperkar: methodology, investigation, writing – review and editing, conceptualization, validation, supervision. Pratap Bahadur: validation, supervision, review and editing.

Conflicts of interest

There are no conflicts to declare.

Acknowledgements

V. K. acknowledges the Department of Chemistry, Sardar Vallabhbhai National Institute of Technology (SVNIT), Gujarat, for providing the instrumentation facility. The authors also sincerely acknowledge Dr Kulbir Singh, Department of Chemistry, StFX University, Antigonish, Nova Scotia, Canada for the spectral analysis. K. R. M. K. acknowledges support from the National Science Foundation under Grant No. CHE-1665157, the Wichita State University Department of Chemistry and Fairmount College of Liberal Arts and Sciences; computational resources funded by the National Science

Foundation under Award no. EPS-0903806 and matching support from the State of Kansas through the Kansas Board of Regents; and the National Institute of General Medical Sciences (P20 GM103418) from the National Institutes of Health. The content is solely the responsibility of the authors and does not necessarily represent the official views of the National Institute of General Medical Sciences or the National Institutes of Health

References

- 1 J. Cross and E. J. Singer, *Cationic surfactants: analytical and biological evaluation*, CRC Press, 2019.
- V. Kumar, N. Pal, A. K. Jangir, D. L. Manyala, D. Varade,
 A. Mandal and K. Kuperkar, *Colloids Surf.*, A, 2020, 588,
 124362–124368.
- 3 L. Y. Zakharova, T. N. Pashirova, S. Doktorovova, A. R. Fernandes, E. Sanchez-Lopez, A. M. Silva, S. B. Souto and E. B. Souto, Int, *J. Mol. Sci.*, 2019, 20, 5534–5564.
- 4 T. H. Ito, P. C. Miranda, N. H. Morgon, G. Heerdt, C. A. Dreiss and E. Sabadini, *Langmuir*, 2014, **30**, 11535–11542.
- 5 N. R. Agrawal, X. Yue, Y. Feng and S. R. Raghavan, *Langmuir*, 2019, 35, 12782–12791.
- 6 Z. Chu, C. A. Dreiss and Y. Feng, Chem. Soc. Rev., 2013, 42, 7174–7203.
- 7 D. L. Fredell, *Biological properties and applications of cationic surfactants*, CRC Press, Boca Raton, 1994.
- 8 H. Yin, P. Zheng, J. Zhao and W. Shen, *Soft Matter*, 2017, **13**, 5888–5896.
- 9 T. Shikata, Y. Sakaiguchi, H. Uragami, A. Tamura and H. Hirata, *J. Colloid Interface Sci.*, 1987, **119**, 291–293.
- 10 M. K. Mullally, M. J. Doyle and D. G. Marangoni, *Colloid Polym. Sci.*, 2004, 283, 335–339.
- 11 W. Fatma, S. Khatoon, Z. A. Khan and A. Z. Naqvi, *J. Chem. Eng. Data*, 2008, 53, 2291–2300.
- 12 C. Kennedy, S. MacMillan, M. McAlduff and D. Marangoni, *Colloid Polym. Sci.*, 2001, **279**, 1–7.
- 13 B. E. Hawrylak and D. G. Marangoni, Can. J. Chem., 1999, 77, 1241–1244.
- 14 J. S. Cohen, Trends Biochem. Sci., 1987, 12, 133-135.
- 15 L. W. Kelts, C. J. Landry and D. M. Teegarden, *Macromolecules*, 1993, **26**, 2941–2949.
- 16 K. Kuperkar, A. Patriati, E. Putra, K. Singh, D. Marangoni and P. Bahadur, *Can. J. Chem.*, 2012, **90**, 314–320.
- 17 S. Chavda, K. Singh, M. Perry, D. Marangoni, V. Aswal and P. Bahadur, *Colloids Surf.*, A, 2011, 378, 79–86.
- 18 B. S. Rauniyar and A. Bhattarai, *J. Mol. Liq.*, 2021, 323, 114604–114612.
- 19 E. Hirsch, S. Candau and R. Zana, *J. Colloid Interface Sci.*, 1984, **97**, 318-326.
- 20 L. Sreejith, S. Parathakkat, S. M. Nair, S. Kumar, G. Varma, P. A. Hassan and Y. Talmon, *J. Phys. Chem. B*, 2011, 115, 464–470.
- 21 T. Tomi, T. Maeda, I. Satake and K. Hayakawa, *Colloids Surf.*, *A*, 2009, **346**, 28–33.

PCCP

22 S. Chavda, K. Singh, D. Gerrard Marangoni, V. K. Aswal and P. Bahadur, *J. Surfactants Deterg.*, 2012, **15**, 317–325.

- 23 S. Chavda and P. Bahadur, J. Mol. Liq., 2011, 161, 72-77.
- 24 A. González-Pérez, J. Galán and J. Rodriguez, *Fluid Phase Equilib.*, 2004, **224**, 7–11.
- 25 M. del Mar Graciani, A. Rodríguez, V. I. Martín and M. L. Moyá, *J. Colloid Interface Sci.*, 2010, 342, 382–391.
- 26 I. A. Khan, R. Mohammad, M. S. Alam and Kabir-ud-Din, J. Dispers. Sci. Technol., 2009, 31, 129–137.
- 27 M. Peng, T. T. Duignan, C. V. Nguyen and A. V. Nguyen, *Langmuir*, 2021, 37, 2237–2255.
- 28 R. Verma, A. Mishra and K. R. Mitchell-Koch, J. Chem. Theory Comput., 2015, 11, 5415-5425.
- 29 X. Jia, J. Chen, B. Wang, W. Liu and J. Hao, *Colloids Surf.*, *A*, 2014, 457, 152–159.
- 30 E. Piotrovskaya, A. Vanin and N. Smirnova, *Mol. Phys.*, 2006, 104, 3645–3651.
- 31 B. Kanoje, S. Padshala, J. Parikh, S. K. Sahoo, K. Kuperkar and P. Bahadur, *Phys. Chem. Chem. Phys.*, 2018, **20**, 670–681.
- 32 V. Kumar, D. Patel, H. Pal and K. Kuperkar, *Phys. Chem. Chem. Phys.*, 2019, 21, 15584–15594.
- 33 V. Aswal and P. Goyal, Curr. Sci., 2000, 79, 947-953.
- 34 K. Kuperkar, L. Abezgauz, D. Danino, G. Verma, P. Hassan, V. Aswal, D. Varade and P. Bahadur, *J. Colloid Interface Sci.*, 2008, 323, 403–409.
- 35 J. Hayter and J. Penfold, Colloid Polym. Sci., 1983, 261, 1022-1030.
- 36 V. Patel, D. Ray, K. Singh, L. Abezgauz, G. Marangoni, V. K. Aswal and P. Bahadur, *RSC Adv.*, 2015, **5**, 87758–87768.
- 37 J. M. Martínez and L. Martínez, J. Comput. Chem., 2003, 24, 819-825.
- 38 N. Schmid, A. P. Eichenberger, A. Choutko, S. Riniker, M. Winger, A. E. Mark and W. F. van Gunsteren, Eur. Biophys. J., 2011, 40, 843–856.
- 39 A. K. Malde, L. Zuo, M. Breeze, M. Stroet, D. Poger, P. C. Nair, C. Oostenbrink and A. E. Mark, J. Chem. Theory Comput., 2011, 7, 4026–4037.

- 40 M. Stroet, B. Caron, K. M. Visscher, D. P. Geerke, A. K. Malde and A. E. Mark, *J. Chem. Theory Comput.*, 2018, 14, 5834–5845.
- 41 M. J. Abraham, T. Murtola, R. Schulz, S. Páll, J. C. Smith, B. Hess and E. Lindahl, *SoftwareX*, 2015, 1, 19–25.
- 42 J. C. Roy, M. N. Islam and G. Aktaruzzaman, *J. Surfactants Deterg.*, 2014, 17, 231–242.
- 43 J. Narayanan, C. Manohar, D. Langevin and W. Urbach, *Langmuir*, 1997, 13, 398–401.
- 44 K. Thakkar, B. Bharatiya, D. Ray, V. Aswal and P. Bahadur, J. Mol. Liq., 2017, 241, 136–143.
- 45 T. Deepti, K. K. Ghosh, N. Barbero, P. Quagliotto and G. Soumen, *Colloids Surf.*, A, 2011, 381, 61–69.
- 46 S. Padasala, S. Chavda, D. Ray, V. K. Aswal and P. Bahadur, I. Mol. Lig., 2017, 242, 484–491.
- 47 K. Thakkar, B. Bharatiya, D. O. Shah, D. Ray, V. K. Aswal and P. Bahadur, *Colloids Surf.*, *A*, 2015, **484**, 547–557.
- 48 D. R. Lide, CRC Handbook of Chemistry and Physics, 2005.
- 49 M. del Mar Graciani, A. Rodríguez, M. Muñoz and M. L. Moyá, *Langmuir*, 2005, **21**, 7161–7169.
- 50 M. Almgren and S. Swarup, *J. Colloid Interface Sci.*, 1983, **91**, 256–266.
- 51 H. Singh and S. Swarup, *Bull. Chem. Soc. Jpn.*, 1978, **51**, 1534–1538.
- 52 C. McMahon, B. Hawrylak, D. G. Marangoni and R. Palepu, *Langmuir*, 1999, 15, 429–436.
- 53 G. F. Catá, H. C. Rojas, A. P. Gramatges, C. M. Zicovich-Wilson, L. J. Álvarez and C. Searle, *Soft Matter*, 2011, 7, 8508–8515.
- 54 V. Kumar, G. M. Sai, R. Verma, K. R. Mitchell-Koch, D. Ray, V. K. Aswal, P. Thareja, K. Kuperkar and P. Bahadur, *Lang-muir*, 2021, 37, 4611–4621.
- 55 V. Lutz-Bueno, S. Isabettini, F. Walker, S. Kuster, M. Liebi and P. Fischer, *Phys. Chem. Chem. Phys.*, 2017, **19**, 21869–21877.